Surface Modifications of Biomedical Gum-Metal-Type Alloy by Nano Surface—Severe Plastic Deformation

DOINA RADUCANU,[1] VASILE DANUT COJOCARU,[1]
ANNA NOCIVIN [ID],[2,3] ION CINCA,[1] NICOLAE SERBAN,[1]
and ELISABETA MIRELA COJOCARU[1]

1.—Faculty of Materials Science and Engineering, POLITEHNICA University of Bucharest, 060042 Bucharest, Romania. 2.—Faculty of Mechanical, Industrial and Maritime Engineering, Ovidius University of Constanta, 900527 Constanta, Romania. 3.—e-mail: anocivin@univ-ovidius.ro

For developing performant metallic materials for medical implants, biomechanical adaptation is important for both the bulk material and the material's surface. Therefore, a nano surface-severe plastic deformation (NS-SPD) treatment was applied on the surface of a gum-type alloy (Ti-Nb-Zr-Fe-O) with enhanced bulk mechanical biocompatibility. Six variants with different processing parameters were tested using small impact balls accelerated by compressed air. Before the NS-SPD treatment, the alloy was first subjected to thermomechanical processing to achieve a high compositional and structural homogeneity and proper mechanical properties of the core structure. A detailed microstructural analysis was performed on the thermomechanical-processed alloy and on the surface areas. The microstructural analysis (based on scanning electron microscopy electron backscatter diffraction and x-ray diffraction) reveals the influence of the NS-SPD treatment by formation of two different surface layers: an outer, very thin layer, approximately 10 μm in width, formed of titanium oxides as a consequence of surface oxidation during ball impacts in an air atmosphere, and one approximately 100 μm to 250 μm in width, representing a zone of high-density microstructural defects.

INTRODUCTION

The gradually growing demands for improved materials designed for performant, long-life, hard-tissue implants are well known.[1] Among all metallic biomaterials used at this moment, β-titanium alloys have received much attention because of their proved advantages for the following two important directions: (1) mechanical biocompatibility, ensured by a low elastic modulus whose values are close to those of human cortical bone, combined with high-strength and high-fatigue resistance; and (2) biochemical compatibility, such as high corrosion resistance and good biocompatibility.[1,2] However, for all hard-tissue implants, including the β-Ti alloy implants, one of the most important problems requiring improvement is the surface status,[3,4] because the failure of the implants usually starts at the surface as a result of fretting, wear, fatigue, and corrosion.[5] Often, the problems of the β-type titanium alloy implants appear when the implant surface is encapsulated by fibrous tissue without producing any osseous junctions with surrounding tissues after implantation.[6] For an improved osteointegration of the titanium alloys, it is necessary to obtain durable surfaces, processed on to the implant alloy, capable of preventing any cracking or exfoliations, coupled with a proper roughness for a rapid and durable osseous integration.[7–9] Therefore, the improvement of implant surface properties has a high demand in actual research programs.

Among many possible surface treatments, a new and promising way of improving the surface's characteristics is generically named *nano surface– severe plastic deformation* (NS-SPD),[10–12] which represents a new family of severe plastic deformation (SPD) processes, such as ultrasonic shot peening,[13] high-energy shot peening,[14] surface mechanical attrition treatment,[9] and surface nanocrystallization and hardening,[15] developed to generate on the metallic material surface a nanocrystalline or at least an ultrafine-grain surface

layer. Thus, the locally applied SPD process consists of surface micro-deformations generated through repeated impacts of high-velocity balls or shots, at high strain rates of approximately 10^2 s^{-1} to 10^3 s^{-1}, without alloy chemical composition changing,[16,17] as in many other surface processing methods (physical vapor deposition, chemical vapor deposition, sputtering, etc.). Also, the resulting surface structure is porosity and impurity free. Beneath the NS-SPD surface, deep compressive residual stresses are generated, which creates a superficial self-nano-crystallized structure, for which the applied processing parameters have a direct effect on the plastically deformed microvolumes at the surface. The effects are on local topography and microstructure, being created conditions for new phenomena developing at a crystalline grain level and crystal lattice level/atomic level in the superficial layers.

NS-SPD treatment has been successfully applied more often on such types of material as AISI 316L stainless steel,[9,18] and some attempts on Cu,[19] Cu-30Ni,[20] Al-Si,[21] alloy 718,[22] and cp-Ti.[23] For NS-SPD applied on β-type titanium alloys, there are only few reports, incipient but promising, that refer to Ti-Nb-Zr-Fe[3,6] and Ti-Nb-Mo-Zr-Sn[24] compositions only. It is well-known that, among all β-Ti alloys used for hard-tissue implants, the most appreciated are Ti-Nb-Ta-Zr (TNTZ) composition types because of their suitable combination of mechanical and biomedical functional properties.[25–29] In solution-treated condition, the bulk TNTZ alloys have a desirable low elastic modulus, approximately 55 GPa, but with not so high strength, generally not exceeding 550 MPa, which may be insufficient for hip implant applications.[30] Therefore, the strengthening modality of these TNTZ alloys in bulk condition is the oxygen addition (TNTZ-O—*gum metal*), already applied; oxygen acts like an interstitial strengthening element and inhibits the stress-induced-martensitic (SIM) transformation.[31,32] Another strengthening modality of the bulk alloy is by thermomechanical processing, which involves grain refining to ultrafine or even nanometer dimensions.[33] The scientific research in the present work proposes to cumulate the effects of applying the NS-SPD treatment on the surface of a gum-metal-type alloy that was first thermo-mechanically processed in a bulk condition. The purpose of this approach is to obtain an improved bioalloy, with performant properties in the core volume and at the surface as well. The *gum metal* investigated in this study was developed previously;[34] in this study, after a preliminary thermomechanical treatment for the alloy core performance, the NS-SPD surface treatment was performed in a few different parametrical variants for the purpose of obtaining modified, performant surface characteristics.

The structural and mechanical characteristics of the core material were investigated, as well as the surface characteristics and microstructural evolution in the function of the NS-SPD applied variant.

MATERIALS AND METHOD

Gum-Type Alloy Synthesis

The nominal composition of the tested alloy (Ti-Nb-Zr-Fe-O) was 31.7% Nb, 6.21% Zr, 1.4%Fe, 0.16%O, balance of Ti (mass fraction). The alloy was obtained using a levitation induction melting furnace FIVE CELES—MP25 with a nominal power of 25 kW and a melting capacity of 30 cm^3 under a high vacuum of 10^{-4}–10^{-5} mbar protective atmosphere. The alloy synthesis was made under a high vacuum and intense agitation of the melted alloy with remelting of the ingots done twice to obtain a high degree of chemical homogeneity.

Thermo-mechanical Processing (TMP) of the Ti-Nb-Zr-Fe-O Alloy

After the synthesis process and before the NS-SPD treatment, the as-cast alloy was processed by a preliminary, specific TMP (Fig. 1) consisting of (1) a homogenization treatment (HT) at 1223 K (950°C) with a holding time of approximately 360 min/water quenching (w.q.), using a GERO SR 100 × 500 type of oven under high vacuum; (2) a cold rolling (CR) with a relative reduction, $\varepsilon = 65\%$, using a Mario di Maio LQR120AS rolling mill with 3 m/min rolling speed, without any lubrication; before the CR process, the samples were cleaned using an ultrasonic bath at 60°C in ethyl alcohol; and (III) a solution treating at 1123 K (850°C) with a holding time of approximately 15 min/w.q., using the same oven type as for HT.

NS-SPD Treatment of the Ti-Nb-Zr-Fe-O Alloy Surface

The application of the NS-SPD treatment on the surface of a gum-metal-type alloy has not been reported. Therefore, the intention in this study was an exploration/screening of the processing parameters of the NS-SPD treatment to find a suitable combination for performant results. This exploring process starts from two important data for this kind of experiment acquired on other types of titanium alloy: (1) The impact ball diameter varies, usually between 1 and 3 mm for the already tested Ti alloys[35–37] and (2) the total mass of the impact balls is recommended to be no higher than approximately 25% of the chamber volume used for the mechanical surface treatment.[23,35,38,39]

For the present work, three different diameters were selected for the impact balls, made of AISI 316L steel: 1 mm, 1.6 mm, and 2.0 mm. They had a smooth surface, a hardness of approximately 60 HRC, and a density (ρ) of approximately 7.8 g/cm^3. For exploring more experimental variants, for each
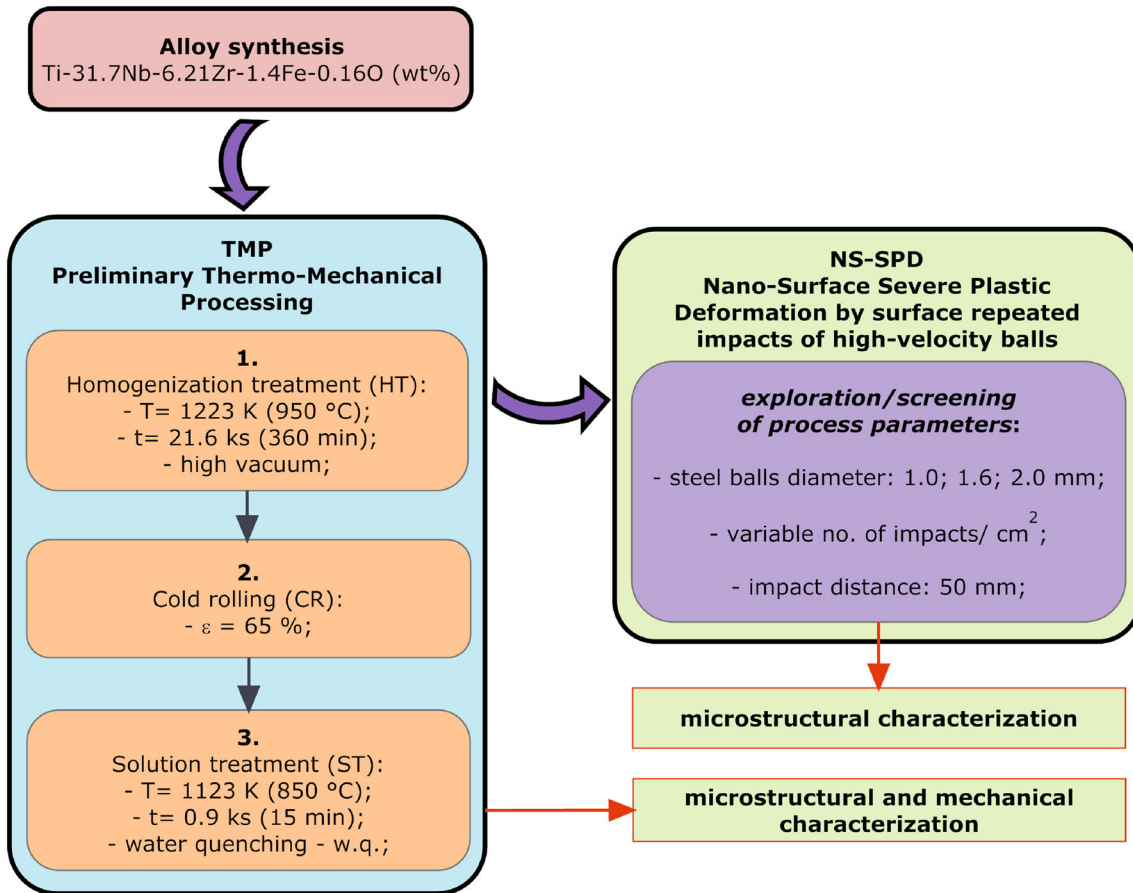
Fig. 1. General scheme of the Ti-31.7Nb-6.21Zr-1.4Fe-0.16O (wt.%) alloy processing.

impact ball diameter, two different ball quantities were used, 3 and 6 kg, resulting in six different experimental variants. To perform the NS-SPD treatment, the sample of $10 \times 60 \times 40$ mm, resulting after the preliminary TMP of the alloy, was cut into six smaller pieces of $2 \times 0.6 \times 40$ mm. The impact balls were accelerated by compressed air (with a flow pressure of 9 atm) being directed perpendicularly on the sample surface. For each NS-SPD variant, the time of the surface mechanical treatment was approximately 20 min, with 50 mm for the ball impact distance. The bombarding input energy E_b of the impact balls depended on ball mass (m_b) and ball velocity (v), $E_b = (m_b v^2/2)$. Thus, for each experimental NS-SPD variant, the number of impacts/cm^2—N—was calculated. Data for all NS-SPD treatment variants are provided in Table I.

Microstructural and Mechanical Analysis

After the NS-SPD treatment, for examining and analyzing the microstructural evolution from the surface in depth to the sample core, all samples were cut in a perpendicular direction to the treated surface to observe the profile in depth of the obtained NS-SPD layer.

A Metkon MICRACUT 200 machine, with diamond cutting disks, was used for this cutting process. Then, the specimens were fixed on a specific epoxy resin of a Buehler SamplKwick type, were abraded with 1200-grit SiC paper using a Metkon Digiprep ACCURA equipment, and finally were mechanically polished using 6 μm, 3 μm, and 1 μm diamond paste and 0.03 μm colloidal silica on Buehler VibroMet2 equipment.

The scanning electron microscopy (SEM) examination of the thermo-mechanically processed alloy (the core microstructure) and of the NS-SPD layers was made using a scanning electron microscope, TESCAN VEGA II—XMU.

The x-ray diffraction (XRD) analysis of the Ti-Nb-Zr-Fe-O alloy, after TMP and after the surface mechanical treatment, was made using a Panalytical X'Pert PRO MRD diffractometer, with Cu k-alpha ($\lambda = 0.15418$ nm) in the range $2\theta = 30°–90°$, using a step size of 0.02°, 40 kV, and 30 mA. The recorded XRD spectra were fitted using the PeakFit v.4.11 software package, to determine for each diffraction peak the position, intensity, and peak-broadening full width at half maximum (FWHM) parameters.

The tensile tests, performed on the thermo-mechanically processed samples, were realized using a

Table I. NS-SPD treatment parameters and the surface layer width of the modified zone (μm)

NS-SPD variant type	Steel ball diameter, Φ (mm)	Total impact ball mass M (Kg)	N—number of impacts (cm^2)	Average surf. layer width after NS-SPD treatment (μm)
V1	1.0	3	150×10^3	110
V2	1.0	6	300×10^3	200
V3	1.6	3	58×10^3	150
V4	1.6	6	116×10^3	180
V5	2.0	3	29×10^3	220
V6	2.0	6	58×10^3	240

Gatan MicroTest-2000N-type machine, with a strain rate of 1×10^{-4} s^{-1}; the following average values of the mechanical characteristics were determined: ultimate tensile strength (σ_{UTS}), yield strength ($\sigma_{0.2}$), elongation to fracture (ε_f), and elastic modulus (E).

RESULTS AND DISCUSSION

Microstructural and Mechanical Characterization of the TMP Alloy

To evaluate the effects on the bulk characteristics of the Ti-Nb-Zr-Fe-O alloy, after the preliminary TMP, which ensured the alloy's biocompatibility and biomechanical adaptation at a macroscale, an energy-dispersive spectroscopy (EDS) and a SEM (secondary electron—SE and back-scattered electron—BSE imaging) analysis were performed. Figure 2 presents a homogeneous distribution of the chemical elements in the TMP sample core. These EDS analyses confirmed the chemical composition of the investigated alloy: Ti-31.7Nb-6.21Zr-1.4Fe-0.16O (mass%).

Some microstructural characteristics of the TMP alloy are presented in Fig. 3. The SEM images of the core microstructure show homogeneous equiaxed ultrafine grains of single β phase with high angle boundaries (Fig. 3a, b and c), with minimal intragranular disorientation (Fig. 3d) and with an average grain dimension of approximately 55.2 μm (Fig. 3e). All grains were randomly oriented without an obvious texture and without twins. Along with Fig. 2, which presents the obtained chemical homogeneity of the TMP alloy, Fig. 3 indicates, in turn, the structural homogeneity of the bulk alloy.

From the tensile tests performed on the samples of Ti-Nb-Zr-Fe-O alloy, in TMP condition, without surface mechanical treatment, the following average values of the mechanical characteristics (Fig. 4) were determined: the ultimate tensile strength $\sigma_{UTS} = 1083 \pm 10.2$ MPa, the yield strength $\sigma_{0.2} = 655 \pm 8.5$ MPa, the elongation to fracture $\varepsilon_f = 9.3 \pm 2.4\%$, and the elastic modulus $E = 61 \pm 2.8$ GPa.

Considering that the studied alloy is intended to be used for the biomedical domain, for which an ultrafine structure with a low modulus of elasticity

is necessary, it can be emphasized, based on the experimental results for the core structure and compared with the characteristics of other gum alloys[27–29,31] that the investigated alloy has the main four important characteristics necessary for good mechanical biocompatibility; the β phase is stable, the crystalline grain dimension is small (approximately 55.2 μm), the ultimate tensile strength is high ($\sigma_{UTS} = 1083$ MPa), and the modulus of elasticity is low (61 GPa).

Microstructural Characterization of the Ti-Nb-Zr-Fe-O Alloy Surface, Treated by NS-SPD

The central aim of the present research is obtaining a mechanically modified surface on a gum metal alloy with improved bulk characteristics; at this stage of the research, the major goal is the microstructural characterization of the alloy surface, treated by NS-SPD. The microstructural features are illustrated in Fig. 5a, b, c, d, e and f, which shows cross sections of the surface-treated samples for all six NS-SPD variants used in the experiments. The following characteristics can be identified: The region corresponding to the core structure, shown in Fig. 3, is a deformation-free region, with unchanged equiaxed morphologies of the β phase, similar to the initial alloy structure before the NS-SPD treatment. After the NS-SPD treatment, in the severe plastic-deformed surface region, the formation of two characteristic surface layers, visible in Fig. 5a, b, c, d, e and f, is identified.

1. The first is an outer, very thin layer, of approximately 10 μm in width, almost identical for all six NS-SPD variants, considered to be formed of titanium oxides as a consequence of surface oxidation and passivation during/after the ball impacts in atmospheric air. This layer can be a barrier against outside corrosion or can be mechanically removed. It is well known that the physicochemical and electrochemical properties of the oxide film, as well as its long-term stability in biological environments, play a major role for the biocompatibility of titanium implants.[39]

2. The second layer, much larger than the first one, with a width of approximately 100 μm to
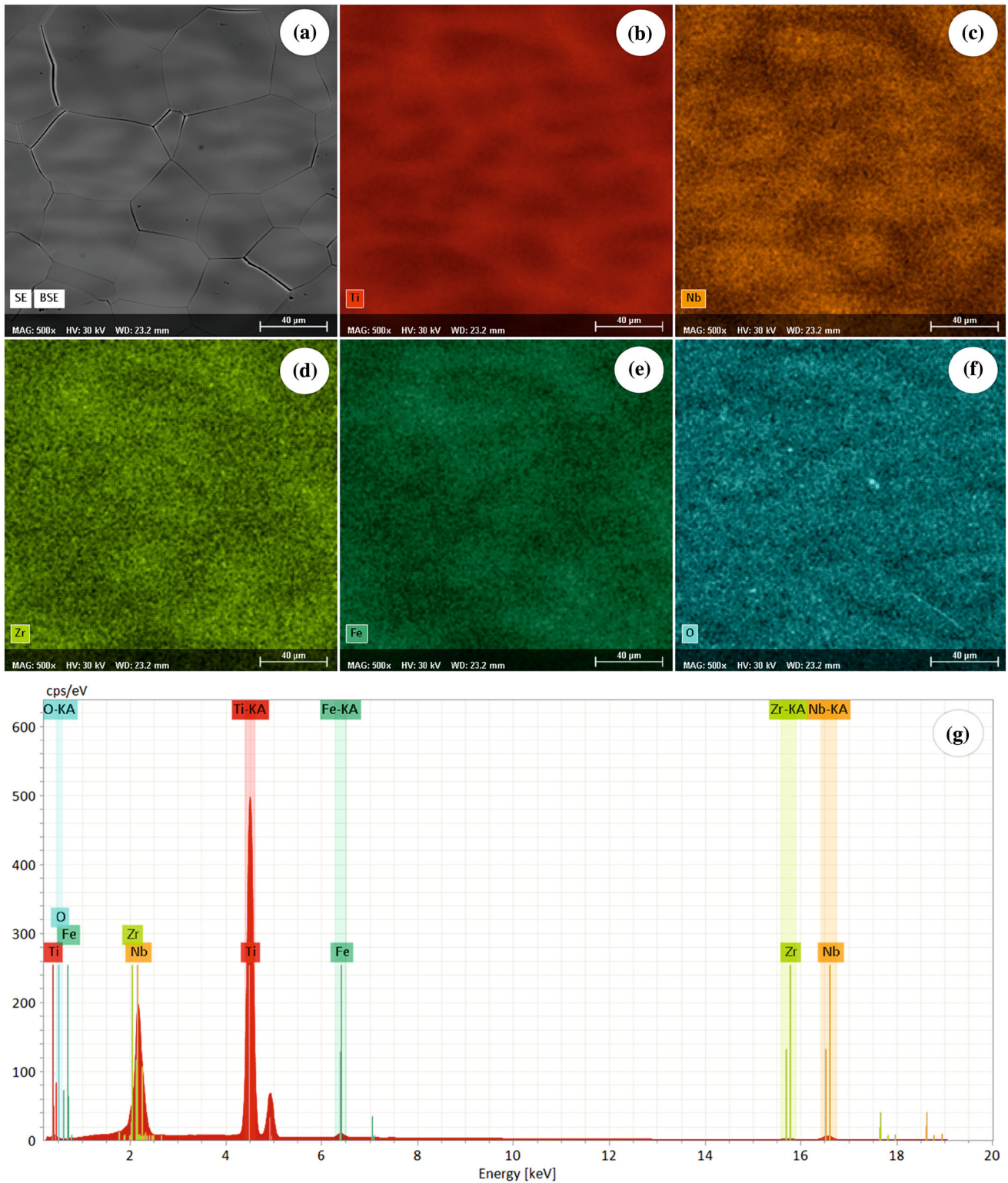
Fig. 2. Chemical elements distribution in the core region of the Ti-Nb-Zr-Fe-O alloy, in the TMP state: (a) the SEM SE-BSE image of the analysed zone; (b) Ti distribution; (c) Nb distribution; (d) Zr distribution; (e) Fe distribution; (f) O distribution; and (g) the EDS spectra of the analysed zone.

250 μm, depending on the NS-SPD applied variant, represents a high-density twin (HDT) zone with possible dislocation bands. The depth of this second layer continuously increases because of the increase of the micro-strain accumulations, depending on the bombarding
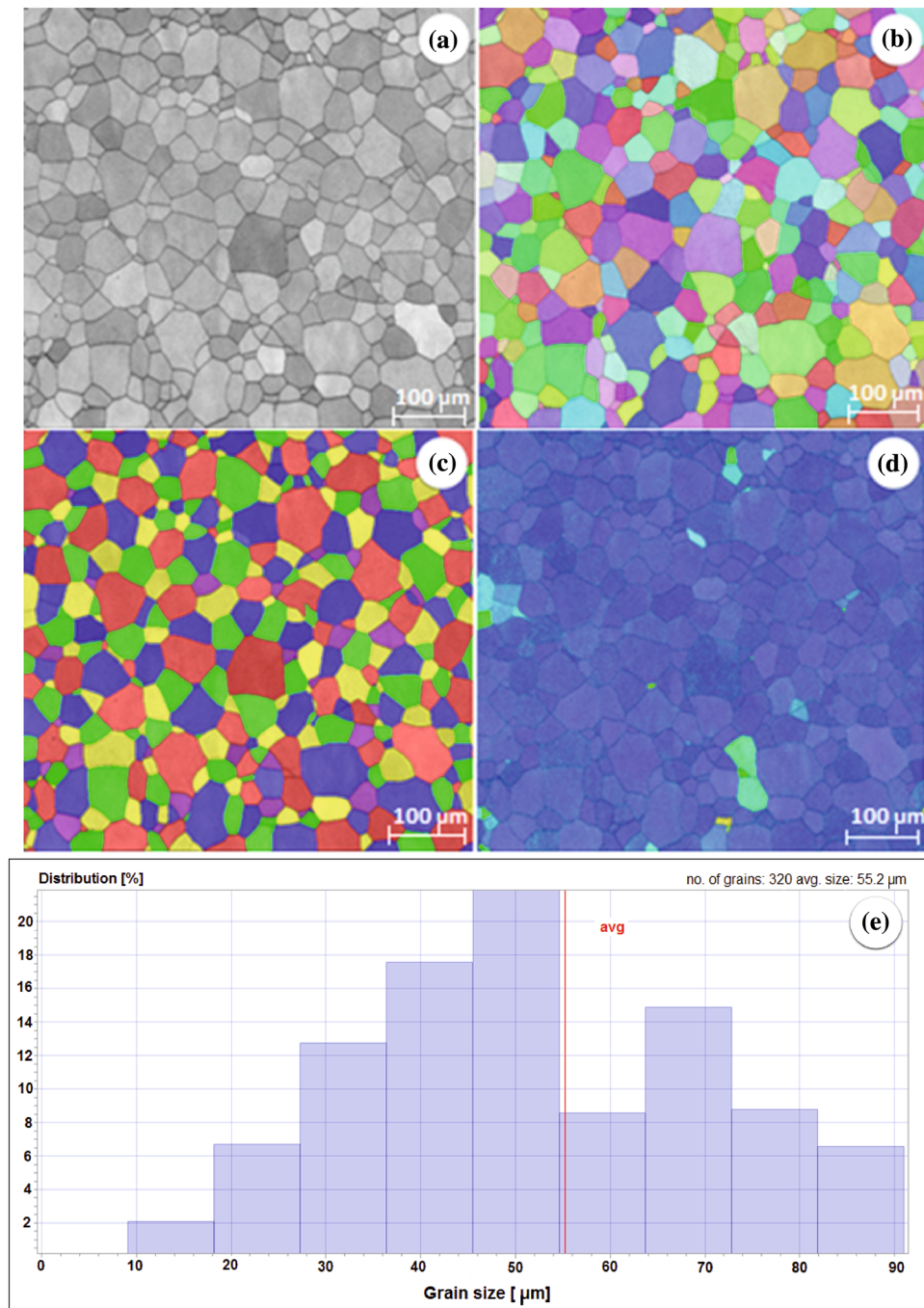
Fig. 3. SEM-EBS images of the Ti-Nb-Zr-Fe-O alloy, in the TMP state: (a) pattern quality map; (b) inverse pole figure (IPF) colour map image; (c) grain size colouring map image; (d) KAM (kernel average misorientation) map image; (e) grain size distribution analysis.

energy of the impact balls, which depends on the balls' mass and the impact ball diameter. This second layer is of maximum interest because it can improve the alloy surface features.

For all NS-SPD variants, the twins in the processed alloy surface are clearly visible in Fig. 5. As a function of both the impact ball diameter and the N (number of impacts/cm^2), the crystallographic changes are more or less pronounced and refer to the twin's formation and possible lattice distortions with dislocation accumulation. With the increase of the impact ball diameter, the area of influence becomes larger (V4–V6 compared with V1–V3). For the same ball diameter (corresponding to the variants V1–V2, V3–V4, and V5–V6), the width of the modified zone is larger for a higher N (Table I). From all six NS-SPD applied variants, the largest
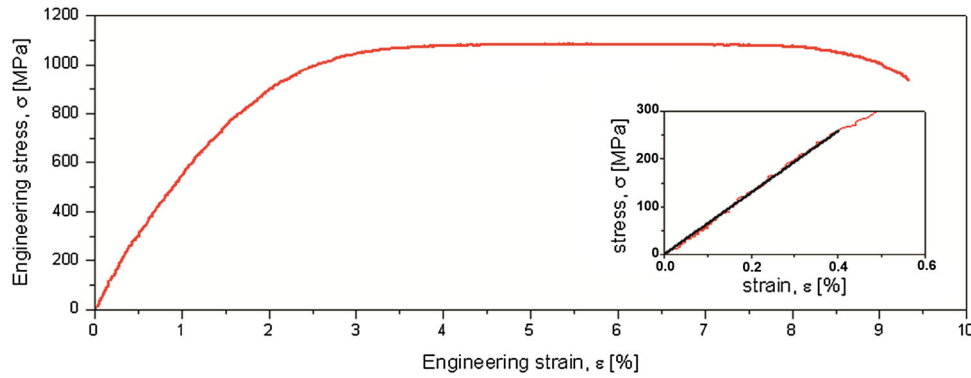
Fig. 4. Stress–strain diagram of the Ti-Nb-Zr-Fe-O alloy in TMP condition (core structure).

modified zone is identified for the NS-SAPD V6 variant, of approximately 240 μm in width, containing the highest density of twins.

In Fig. 6a, b, c, d and e are presented the XRD spectra of the Ti-Nb-Zr-Fe-O alloy in all conditions. Figure 6a shows the alloy in TMP condition, the core structure. Figure 6b, c, d and e shows the alloy after the NS-SPD treatment (V1–V6).

All XRD spectra, which indicate the presence of a single β-phase with clearly contoured diffraction peaks of the crystallographic structure, confirm that the NS-SPD treatment does not influence/change the phase nature of the core material. However, after analyzing the peak's position, intensity, and broadening in all XRD spectra, some comments are necessary. The diffraction peaks of the β-phase corresponding to the core structure of the alloy (Fig. 6a) are relatively sharp. The XRD spectra of the surface-treated samples (Fig. 6b, c and d) are pair-grouped for the NS-SPD variants (V1–V2; V3–V4; V5–V6) corresponding to the experiments realized with the same impact ball diameter but with two different N (number of impacts/cm^2). The overall characteristic of these XRD patterns is their apparent similarity. Inside the explored scattering domain, some similarities are observed concerning the peaks' sequence and position; however, significant differences are observed concerning the peak broadening and intensity. Generally, the broadening of the Bragg diffraction peaks is a result of the lattice distortion of the heavily distorted grains and/or of the grain refinement.

For the present case, there is a visible broadening of the diffraction peaks (especially for the V1, V2, and V6 variants) after applying the NS-SPD treatment compared with the initial core structure.

For the NS-SPD pair variants V1 and V2, realized by using the same impact ball diameter, the XRD spectra were not significantly modified if the N (number of impacts/cm^2) was considered. Almost identical spectra were observed (Fig. 6b). However, the N (number of impacts/cm^2) influences the peak broadening and intensity for the V3–V6 NS-SPD variants (Fig. 6c, d and e). A half diminution of the diffraction peak of the β-Ti (110) plane for the V6

variant compared with the V5 variant (Fig. 6d) was present. The same comment is also valid for Fig. 6e, which compares the XRD spectra of the alloy core structure with the XRD spectra for the treated alloy in the V6 variant. Therefore, the most indicated NS-SPD variant from all those studied is V6, capable of inducing crystallographic changes in the material surface, in terms of lattice distortions and/or grain refinement. This observation must be correlated with information from Fig. 5f, which shows the largest HDT zone for the V6 NS-SPD variant. Thus, for the V6 NS-SPD variant, the SPD-treated zone is the largest and has the highest twin density and possibly other crystallographic changes affecting the fine structure, which represents the most probable premise for initiating the process of grain refinement due to the development of the severe plastic deformation process, if considering the grain refinement mechanism discussed previously[38–40] and schematized for the present case in Fig. 7.

Figure 7 indicates that, through the present NS-SPD experiments, only an exploratory part of the surface nano-crystallization process that could be developed by NS-SPD until the stage corresponding to high accumulation in the surface structure of crystallographic changes identified by twins, lattice distortions, and possible dislocation bands has been investigated. In the future, NS-SPD experiments should continue to be investigated deeply by advanced tools (crystalline structure determination and data concerning the crystalline zones, lattice parameters, micro strains, and crystal orientation) to determine the influence of NS-SPD processing parameters on the fine structure of the gum metal alloy, with practical consequences for the microhardness characteristics, corrosion behavior, and wear resistance of the processed/modified surface.

CONCLUSION

- The scientific approach of this study was applying NS-SPD processing on the surface of a gum-metal-type alloy (Ti-Nb-Zr-Fe-O) for modifying the surface characteristics/microstructure. For
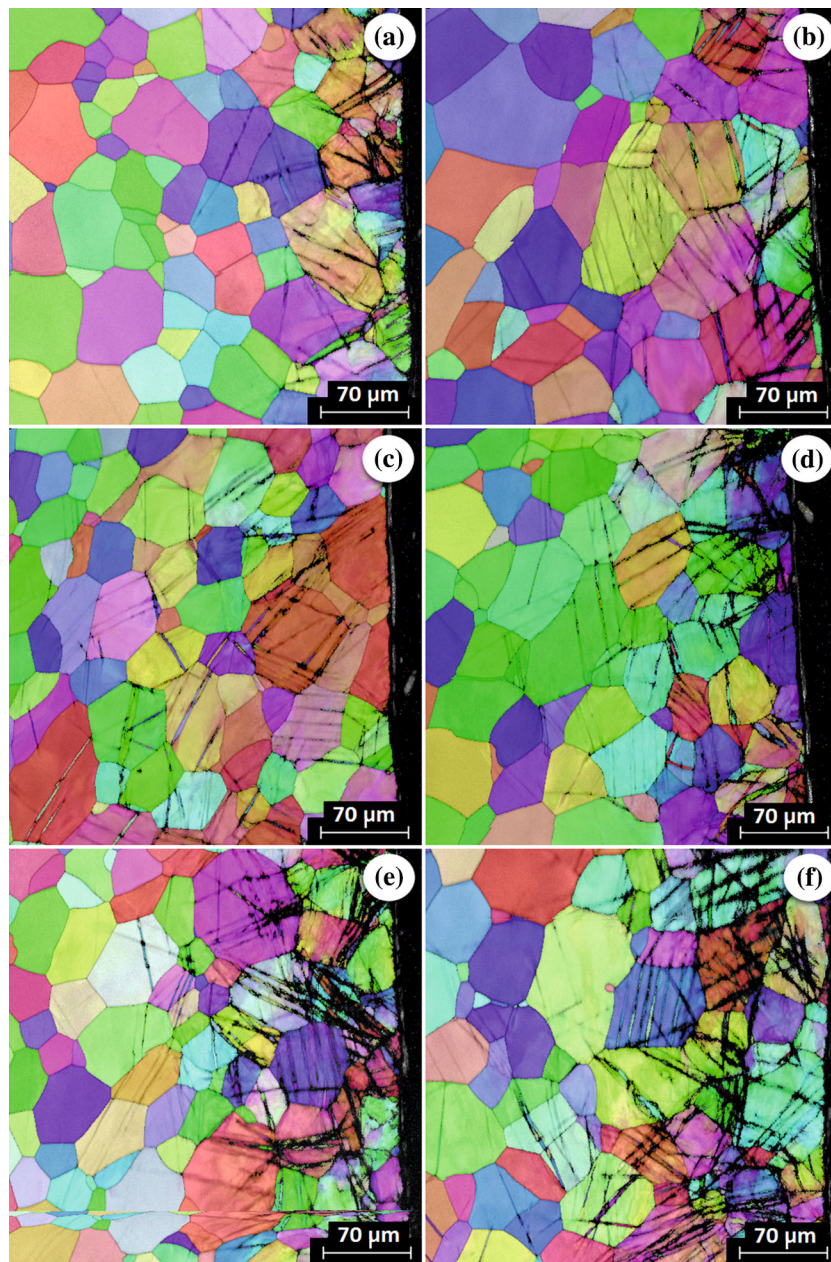
Fig. 5. SEM images of the Ti-Nb-Zr-Fe-O alloy after the NS-SPD treatment: (a) V1; (b) V2; (c) V3; (d) V4; (e) V5; (f) V6; for all variants, the outer thin layer of titanium oxides and HDT (*high density of twin*) zone are visible.

the Ti-Nb-Zr-Fe-O alloy, performant properties in core volume were obtained through a thermo-mechanical process, applied preliminarily in a bulk condition.

- The alloy in the TMP condition has the characteristics necessary for good mechanical biocompatibility: The β phase is stable, the crystalline grain dimension is small (approximately 55.2 μm), the ultimate tensile strength is high (σ_{UTS} = 1083 MPa), and the modulus of elasticity is low (61 GPa).

- Surface layers, with plastically deformed micro-volumes, were realized after applying different variants of NS-SPD mechanical treatment, on

the Ti-Nb-Zr-Fe-O alloy. An exploration/screening of the NS-SPD processing parameters to find a suitable combination for significant results in terms of crystallographic surface modifications was realized by the variation of the impact ball diameter (1.0, 1.6, and 2.0 mm) and of the applied N (number of impacts/cm^2) for a constant treatment time.

- For all applied NS-SPD treatment variants, the modified surface area had a high twin density and lattice distortion/heavily distorted grains, indicated by the XRD spectra profile.

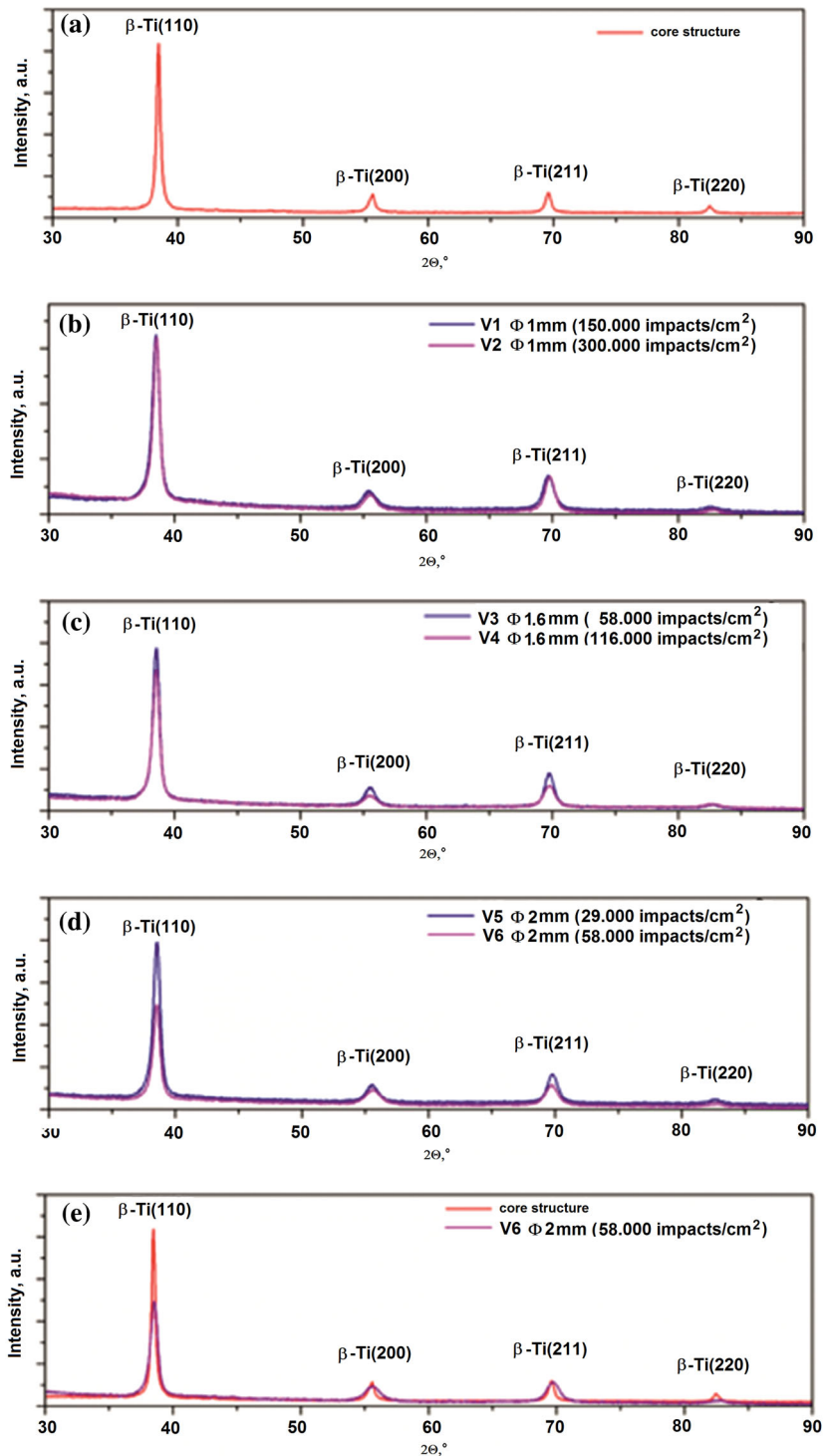- Of all applied NS-SPD treatment variants, the most promising is the NS-SPD V6 variant (im-

Fig. 6. XRD spectra of the Ti-Nb-Zr-Fe-O alloy: (a) core structure; (b) V1 and V2 of the NS-SPD treated alloy; (c) V3 and V4 of the NS-SPD treated alloy; (d) V5 and V6 of the NS-SPD treated alloy; (e) core structure and V6—NS-SPD treated alloy.

pact ball diameter of 2 mm and 58,000 impacts/cm^2), for which the largest surface-influenced zone was obtained, of approximately 240 μm width and with the highest twin density.

- Further studies are envisaged that will use advanced tools to determine the impact of this NS-SPD treatment on the fine structure of the gum metal alloy able to modify/improve overall characteristics, such as the micro-hardness, corrosion, and wear resistance of the Ti-Nb-Zr-Fe-O alloy.
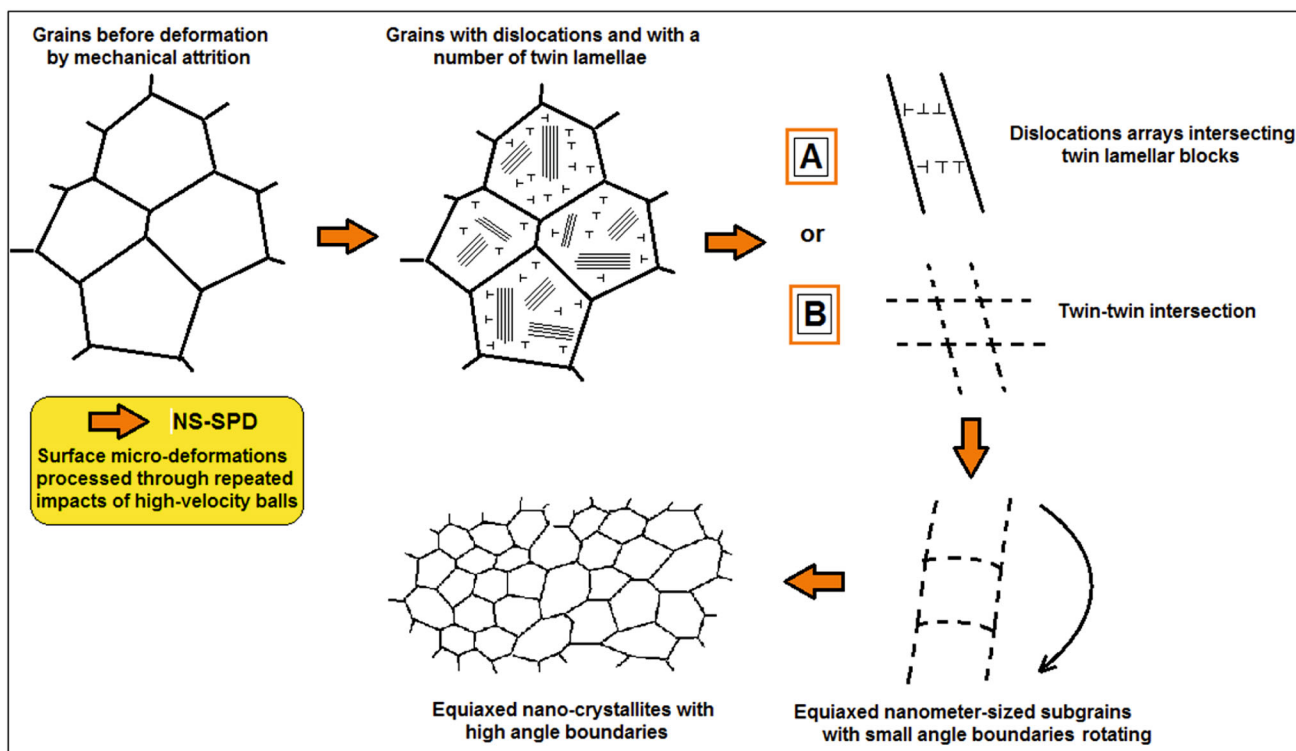
Fig. 7. Schematic illustration of possible grain refinement process during NS-SPD for an alloy having a solid solution structure type: the case of the studied Ti-Nb-Zr-Fe-O alloy core structure.

ACKNOWLEDGEMENTS

REFERENCES

1. M. Abdel-Hady Gepreel and M. Niinomi, *J. Mech. Behav. Biomed. Mater.* 20, 407 (2013).
2. K.Y. Xie, Y. Wang, Y. Zhao, L. Chang, G. Wang, Z. Chen, Y. Cao, X. Liao, E.J. Lavernia, R.Z. Valiev, B. Sarrafpour, H. Zoellner, and S.P. Ringer, *Mater. Sci. Eng. C* 33, 3530 (2013).
3. L. Jin, W. Cui, X. Song, and L. Zhou, *Appl. Surf. Sci.* 347, 553 (2015).
4. X.Y. Liu, P.K. Chu, and C.X. Ding, *Mater. Sci. Eng. R* 47, 49–121 (2004).
5. C. Vasilescu, S.I. Drob, E.I. Neacsu, and J.C. Mirza Rosca, *Corros. Sci.* 65, 431 (2012).
6. L. Jin, W. Cui, X. Song, G. Liu, and L. Zhou, *Trans. Nonferrous Met. Soc. China* 24, 2529 (2014).
7. M.T. Mohammed, Z.A. Khan, and A.N. Siddiquee, *Procedia Mater. Sci.* 6, 1610 (2014).
8. L. Saldana and N. Vilaboa, *Acta Biomater.* 6, 1649 (2010).
9. B. Arifvianto, O. Suyitn, and M. Mahardika, *J. Appl. Surf. Sci.* 258, 4538 (2012).
10. Z. Husaain, A. Ahmed, O.M. Irfan, and F. Al-Mufadi, *Int. J. Eng. Technol.* 9, 426 (2017).
11. M. Aliofkhazraei and A.S. Rouhaghdam, *J. Nanosci. Nanotechnol.* 10, 4777 (2010).
12. A.I. Yurkova, Y.V. Milman, and A.V. Byakova, *Russ. Metall.* 2010, 258 (2010).
13. M. Rakita, M. Wang, Q. Han, Y. Liu, and F. Yin, *Int. J. Comput. Mater. Sci. Surf. Eng.* 5, 189 (2013).
14. H. Wang, X. Yuan, K. Wu, C. Xu, Y. Jiao, W. Ge, and J. Luo, *J. Mater. Process. Technol.* 255, 76 (2018).
15. G. Zhao, A.L. Raines, and M. Wieland, et al., *Biomaterials* 28, 2821 (2007).
16. Y. Samih, B. Beausir, B. Bolle, and T. Grosdidier, *Mater. Charact.* 83, 129 (2013).
17. K.A. Darling, M.A. Tschopp, A.J. Roberts, J.P. Ligda, and L.J. Kecskes, *Scr. Mater.* 69, 461 (2013).
18. S. Bahl, S. Suwas, T. Ungàr, and K. Chatterjee, *Acta Mater.* 122, 138 (2017).
19. R. Blonde, H.L. Chan, N.A. Bonasso, B. Bolle, T. Grosdidiera, and J. Lu, *J. Alloys Compd.* 504, s410 (2010).
20. X. Mao, D. Li, Z. Wang, X. Zhao, and L. Cai, *Trans. Nonferrous Met. Soc. China* 23, 1694 (2013).
21. H.W. Chang, P.M. Kelly, Y.N. Shi, and M.X. Zhang, *Mater. Sci. Eng. A* 530, 304 (2011).
22. S. Anand Kumar, S. Ganesh Sundara Raman, T.S.N. Sankara Narayanan, and R. Gnanamoorthy, *Surf. Coat. Technol.* 206, 4425 (2012).
23. M. Wen, G. Liu, J. Gu, W. Guan, and J. Lu, *Surf. Coat. Technol.* 202, 4728 (2008).
24. R. Huang and Y. Han, *Mater. Sci. Eng. C* 33, 2353 (2013).
25. S. Ozan, J. Lin, Y. Li, and C. Wen, *J. Mech. Behav. Biomed. Mater.* 75, 119 (2017).
26. Y. Zheng, R.E.A. Williams, S. Nag, R. Banerjee, H.L. Fraser, and D. Banerjee, *Scr. Mater.* 116, 49 (2016).
27. Y. Li, C. Yang, H. Zhao, S. Qu, X. Li, and Y. Li, *Materials* 7, 1709 (2014).
28. D. Raducanu, V.D. Cojocaru, A. Nocivin, D.M. Gordin, and I. Cinca, *Mater. Sci. Eng. A* 689, 25 (2017).
29. D. Raducanu, V.D. Cojocaru, A. Nocivin, I. Cinca, N. Serban, and E.M. Cojocaru, *JOM* 71, 264 (2019).
30. I. Kopova, J. Strasky, P. Harcuba, M. Landa, M. Janecek, and L. Bacakova, *Mater. Sci. Eng. C* 60, 230 (2016).
31. M. Niinomi, M. Nakai, M. Hendrickson, P. Nandwana, T. Alam, D. Choudhuri, and R. Banerjee, *Scr. Mater.* 123, 144 (2016).

32. L.S. Wei, H.Y. Kim, and S. Miyazaki, *Acta Mater.* 100, 313 (2015).
33. B. Sulkowski, A. Panigrahi, K. Ozaltin, M. Lewandowska, B. Mikułowski, and M. Zehetbauer, *J. Mater. Sci.* 49, 6648 (2014).
34. A. Nocivin, V.D. Cojocaru, D. Raducanu, I. Cinca, M.L. Angelescu, I. Dan, N. Serban, and M. Cojocaru, *J. Mater. Eng. Perform.* 26, 4373 (2017).
35. W.Y. Tsai, J.C. Huang, Y.J. Gao, Y.L. Chung, and G.R. Huang, *Scr. Mater.* 103, 45 (2015).
36. T.H. De Keijser, J.I. Langford, E.J. Mittemeijer, and A.B.P. Vogels, *J. Appl. Crystallogr.* 15, 308 (1982).
37. S. Jelliti, C. Richard, D. Retraint, T. Roland, M. Chemkhi, and C. Demangel, *Surf. Coat. Technol.* 224, 82 (2013).
38. J. Azadmanjiri, C.C. Berndt, A. Kapoor, and C. Wen, *Crit. Rev. Solid State Mater. Sci.* (2015). https://doi.org/10.1080/10408436.2014.978446.
39. X.Y. Shi, Y. Liu, D.J. Li, B. Chen, X.Q. Zeng, J. Lu, and W.J. Ding, *Mater. Sci. Eng. A* 630, 146 (2015).
40. C.X. Ren, Q. Wang, Z.J. Zhang, Y.K. Zhu, and Z.F. Zhang, *Acta Metallurg. Sin. (Eng. Lett.)* 30, 212 (2017).